Solvent engineering approach via introducing poly (3, 4-ethylene dioxy-thiophene)–poly (styrene sulfonate) (PEDOT:PSS) into photosensitive absorber layer for ambient temperature processed efficient inverted planar perovskite solar cells

Zhiyong Liu[a*], Kaikai Liu[a,], Huihui Wang[b], Sagar M. Jain[c], Junjie Duan[a], Tingwei He[a], Ruimei Fan[d], Jien Yang[a], Hairui Liu[a], Feipeng Zhang[e]

[a] *Department of Physics and Materials Science, Henan Normal University, Henan Key Laboratory of Photovoltaic Materials, Xinxiang 453007, China*

[b] *College of Civil Engineering and Architecture, Jiaxing University, Zhejiang 314001, China*

[C] College of Engineering, Swansea University Bay Campus, Fabian Way, SA1 8EN Swansea, United Kingdom.

[d] *Civil and Environmental Engineering Department, The University of Delaware Newark, DE. 19716.USA*

[e] *Institute of Physics, Henan University of Construction, Pingdingshan 467036, China*

Abstract

The quality of photosensitive absorber layer plays an important role in the performance of organic-inorganic hybrid perovskite solar cells (PSCs). Here, for the first time a classic hole transport material, poly (3, 4-ethylene dioxy-thiophene)-poly (styrene sulfonate) (abbreviated as PEDOT:PSS) was introduced as additive directly into the $CH_3NH_3PbI_{3-x}Cl_x$ perovskite absorber. On controlled fine-tuning of PEDOT:PSS concentration within perovskite resulted into the high-quality films with large crystal grains that ultimately resulted into improved optoelectronic and charge transport properties. Due to the complexation between the PEDOT:PSS and $CH_3NH_3PbI_{3-x}Cl_x$ the defects in the active layer of perovskite as well as the passivation of back-and-front contact recombination occurred that leads to possible trap state healing in bulk as well at interfaces and this resulted into a longer lifetime charge carrier compare to the perovskite film without PEDOT:PSS additives. Solar cells prepared using 1.5 v% PEDOT:PSS and perovskite resulted an improved power conversion efficiency (PCE) of 17.56%. This finding provided a simple way to fabricate efficient planar perovskite solar cells for the commercial applications.

Keywords: Solvent engineering; PEDOT:PSS additives; Complexation; Optoelectronic properties.

1. Introduction

Photovoltaic field has taken by a storm after the recent emergence of hybrid organic-inorganic lead halide perovskite solar cells. Within a few years' time the organic-inorganic perovskite field is rapidly developed to produce highly efficient certified power conversion efficiency of perovskite devices exceeding 22% (Wu et al., 2017). Moreover, the solution processing and low cost of materials used to prepare solar cells have attracted many researchers to investigate these fascinating materials (Sum et al., 2014; Zhao et al., 2014; Akihiro et al., 2009; Burschka et al., 2013; Chiang et al., 2017). However, there remain some challenges to address such as toxicity of the lead used, long-term stability and low temperature processing of these solar cells, an important factor required for their large-scale manufacturing and commercialization. Perovskite devices are divided into regular configuration and inverted configuration or architecture (Chiang and Wu, 2016). The two-basic architecture representing regular and inverted configurations are fluorine doped on either tin oxide (FTO)/electron transfer layer (ETL)/perovskite/hole transfer layer (HTL)/metal electrode and Indium tin oxide electrode (ITO)/HTL/perovskite/ETL/metal electrode, respectively (Jeon et al., 2014; You et al., 2014). Among two of the above the later configuration of inverted planar perovskite solar cells is of particular importance mainly because of their low-temperature

processing which gives ease for preparation of solar cells on flexible substrate as well for large scale manufacturing. For Inverted device architecture, PEDOT:PSS is widely used as hole transport layer (HTL). However, the use of aqueous conventional processing to deposit PEDOT:PSS makes it challenging to obtained high quality perovskite films required for good performance of solar cells. These important insights should be taken into account when developing efficient and reproducible perovskite solar cells.

It is well-known that the quality of perovskite film has a direct influence on the photovoltaic performance of PSCs (Liu et al., 2017; Jain et al., 2016a, 2016b). There are report of addition of adequate amount of H2O and VOx directly in the perovskite active layer that can alter the morphology and the quality of the perovskite film (Xie et al., 2017; Lee et al., 2012). However, for the PEDOT:PSS HTL due to water processing it becomes challenging to prepare good quality perovskite films. Which is the prime requirement for the high performance solar cells. In this direction, considering this sensitive preparation of good quality perovskite films especially for the low temperature processed (PEDOT:PSS HTL based) inverted perovskite cells. Here, in this work for the first time a classic hole transport material PEDOT:PSS was added directly into the perovskite absorber to fine tune the optoelectronic quality of the perovskite film. This resulted into the formation of good

quality perovskite films, compared to the perovskite films that are prepared without PEDOT:PSS doping.

Interestingly, the morphology of perovskite films improved sequentially with the addition of PEDOT:PSS and on 1.5 v% PEDOT:PSS addition into perovskite the quality of the film improved to obtain >1ɯm large grains with homogeneous coverage. While, the films without PEDOT:PSS doping (0 v% PEDOT:PSS reference films) suffered from smaller perovskite grains with voids. The perovskite devices prepared from doped films with 1.5 v% PEDOT:PSS shown improved open circuit voltage (Voc) of 0.99 V and short circuit current density (Jsc) of 22.4 mA cm^{-2} with a improved fill factor of 78.7% resulting into 17.56% power conversion efficiency for champion devices. While, the solar cells prepared without PEDOT:PSS doping resulted into the lower power conversion efficiency of 14.58%.

2. Experimental

2.1 Materials

Hydrogen iodide (HI), methylamine(CH_3NH_2) and Chlorobenzene(C_6H_5Cl) were purchased from Shanghai Chemical Industry Co. N,N-Dimethyl formamide (anhydrous, amine free; 99.9%) and PbCl2(99.999%) were purchased from Alfa-Aesar. The poly (3, 4-ethylene dioxy-thiophene)–poly (styrene sulfonate) (PEDOT:PSS, 4083, 1.3~1.7

wt% dispersion in H_2O) was purchased from Heraeus (Germany). Powder phenyl-C61-butyric acid methyl ester (PCBM) and 4, 7-Diphenyl-1, 10-phenanthroline (Bphen) were produced in Nichem Fine Technology Co., Ltd. (Taiwan). The bulk ITO glass(10Ω sq^{-1}) was purchased from Fine Chemicals Industry Co., Gyeonggi-do. (Korea).

2.2 Fabrication of the precursor solution

First prepared the co-solvent mixture of DMF and PEDOT:PSS in a clean and dried small vial. Then measured out the DMF solution of desired volume separately into the dried reagent bottles. Then we measured the different volume of PEDOT:PSS using pipette to move into the previous reagent bottles with DMF, and controlled the percentage by volume (0 v%, 0.5 v%, 1.0 v%, 1.5 v%, 2.0 v% respectively). The co-solvent mixture of DMF and PEDOT:PSS is placed on a magnetic stirrer for 30 minutes together to mix it up well at room temperature for 30 min.

Fabrication of the $CH_3NH_3PbI_{3-x}Cl_x$-PEDOT:PSS precursor solution: CH_3NH_3I was synthesized by CH_3NH_2 and HI in an ice bath environment, as reported previously (Lee, et al., 2012). $CH_3NH_3PbI_{3-x}Cl_x$-PEDOT:PSS precursor solution was fabricated by putting the pre-weighed powder of CH_3NH_3I and $PbCl_2$ with a ratio of 3:1 into the respective bottles. Then transferred these bottles into the glove box with N_2 and used the pipettes to measure 1ml of solvents. These bottles are kept on magnetic

stirring apparatus for over-night at 60℃, at a speed of 350 rpm. Before device fabrication, precursor solution had been filtered with the 0.45 μm Polytetrafluoroethylene (PTFE) filters to percolate.

The PCBM and Bphen precursor solution were fabricated in the same way as the $CH_3NH_3PbI_{3-x}Cl_x$-PEDOT:PSS precursor solution in N_2 equipped glove box. The difference is that PCBM and Bphen were dissolved by Chlorobenzene or fresh absolute ethyl alcohol independently.

2.3 Devices fabrication

The 15×13 mm ITO glasses cutted from the bulk ITO glasses, were etched by hydrochloric acid and zinc powder as reported previously (Z. Liu, et al., 2017b), and washed with ITO special cleaning agent in ultrasonic bath for 30 min. Then the etched ITO glasses were rewashed for a further cleaning in deionized water, acetone and ethanol with ultrasound for 20 min. respectively. Before spin-coated solution, in order to enhance the wettability, the washed ITO glasses were dried in an oven and treated in UV-Ozone cleaner for 15 min (Xu, et al., 2017). The hole transfer layer of PEDOT:PSS film was spin-coated onto the ITO substrate at 500 rpm for 10 s and 4500 rpm for 50 s in succession and then annealed at 140 ℃ for 20 min. The substrates with PEDOT:PSS film were transferred into a glovebox to proceed the perovskite film coating. The $CH_3NH_3PbI_{3-x}Cl_x$:PEDOT:PSS precursor solution was spin-coated by the

same method as PEDOT:PSS layer. Perovskite films were annealed at a increased temperature method in the previous report (Bai, et al., 2014). The temperature was gradiently increased from 60 to 100 ℃ at a ramp rate of 10℃/10 min on a heating stage, and then dried at 100 ℃ for 90 min. Afterward, PCBM solution was spin-coated at 2000 rpm for 40 seconds onto the perovskite film and dried at 60 ℃ for 20 min. Next, Bphen solution was deposited by spin-coating at 4000 rpm for 40 seconds on PCBM film without heating. Finally, The silver back contact was thermally deposited onto the Bphen film under vacuum at 4.5×10^{-4} Pa through a shadow mask (mask area of 6.25 mm^2).

2.4 Characterizations

The surface morphology of perovskite films and the cross-section morphology of PSCs were characterized by a field-emission SEM (Quanta 200 FEG, FEI Co.). The atomic force microscope (AFM) images were characterized by an Agilent 5500 SPM system (Agilent Technologies, USA). The crystalline phase and X-ray diffraction (XRD) patterns of perovskite films were characterized by a Rigaku D/MAX-2400 diffractometer. The current density–voltage (J–V) curves were recorded (2400 Series Source Meter, Keithley Instruments) under a simulated Air-Mass (AM) 1.5 sunlight at 100 mW/cm^2 (Newport, Class AAA solar simulator, 94023A-U). The incident-photon-to-current efficiency (IPCE) measurement was measured through a system consisted of xenon lamp, monochromator,

chopper and lock-in amplifier and a calibrated silicon photodetector. UV-Vis absorption was recorded with the Shimadzu UV-2550 spectrometer. The electrochemical impedance spectroscopy (EIS) measurement was conducted on a CHI660C electrochemical work station (Shanghai, China) with 5 mV alternating current (AC) amplitude at a frequency range of 106 Hz to 1 Hz. X-ray photoelectron spectroscopy (XPS) was measured by the usage AXIS Ultra instrument (Kratos UK) at a base pressure of ~ 10^{-8} torr and 295 K. Steady-state photoluminescence (PL) spectra were detected on F-4500 fluorescence spectrometer (Hitachi, Japan) with a photomultiplier tube voltage of 400 V. Time-resolved photoluminescence (TRPL) were measured with Edinburgh Instruments Ltd(FLS980).

3. Results and discussion

3.1 Performance of devices

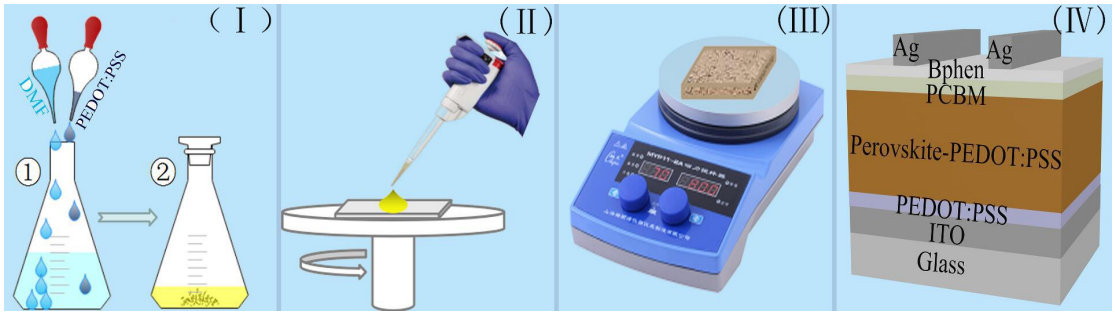

Fig. 1 The schematics of the preparation methodology for inverted PSCs with PEDOT:PSS as additives.

Inverted structure of PSCs consisting ITO/HTL/perovskite/ETL/metal

electrode architecture is studied widely (Hu et al., 2017; Jiang et al., 2017; Gu et al., 2017). Researchers adopted different strategy to enhance the performance of the inverted PSCs by preparing the new materials and some of them have done it by doping in the absorber layer or modifying the functional layers (Kranthiraja et al., 2017; Xu et al., 2017; Wu et al., 2018). As shown in Fig. 1 and stated previously, we introduced the classic hole-transport material PEDOT:PSS into the $CH_3NH_3PbI_{3-x}Cl_x$ perovskite absorber layer by using the mixed solvent of DMF and PEDOT:PSS in aqueous solution with the different volume ratios (0, 0.5, 1.0 ,1.5, 2.0 v%) to fabricate the perovskite precursor solution (refer supplementary Fig. S1). Based on the conventional inverted PSCs, we adopted the conventional spin-coating method to fabricate the different functional layers. A solar cell architecture used is presented in Fig. 1 (IV). The thickness of the photosensitive layer with PEDOT:PSS layer is ≈ 380 nm (figure 5b).

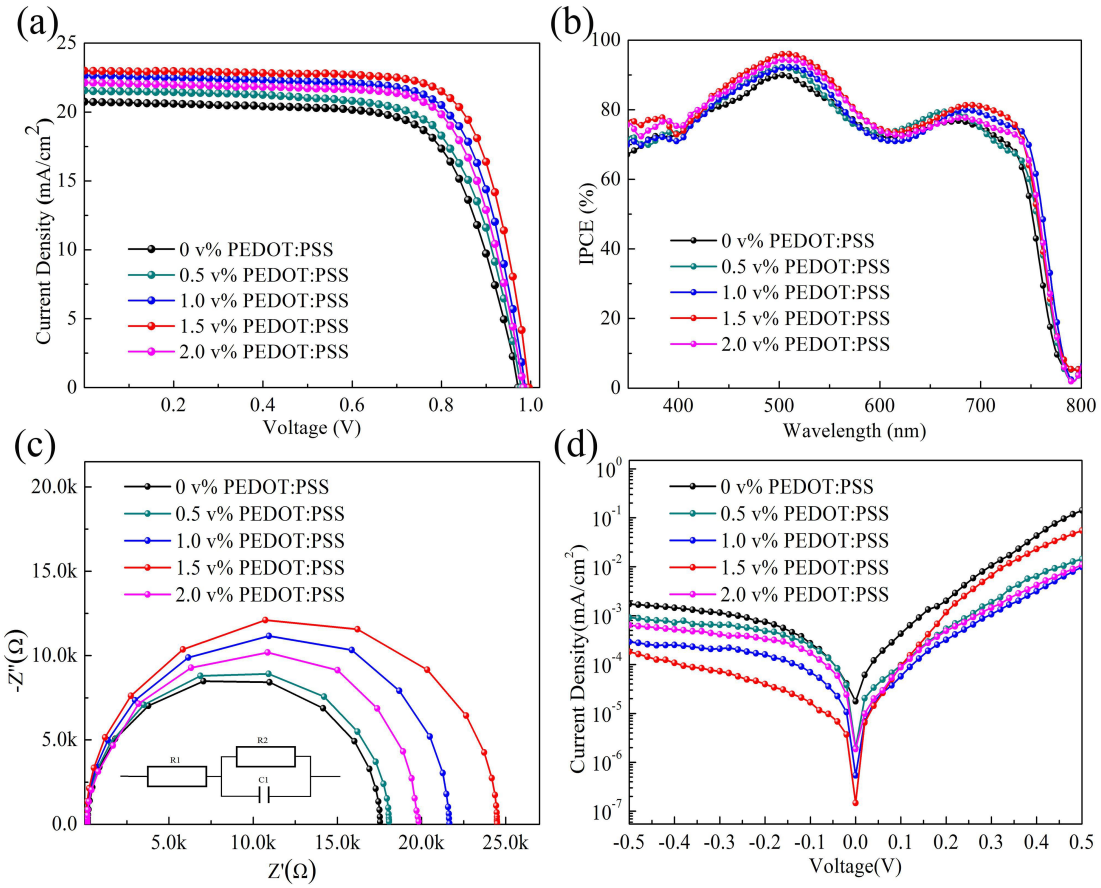

Fig. 2 (a) J-V characteristics, (b) IPCE of the champion devices, (c) Impedance spectroscopy and (d) Dark currents of the PSCs based on perovskite film without the PEDOT:PSS (0 v%) additive (black color) and with the PEDOT:PSS (0.5, 1, 1.5 and 2 v%) additive (red color) respectively.

As PEDOT:PSS HTL due to acidic nature and water processing considered notorious for the deposition of good quality of perovskite films on it. Figure 2a. shows the J-V characteristics of the PSCs based on photosensitive layer of target film and reference film under AM 1.5 G illumination with the light intensity of 1000 Wm^{-2}. Table 1 showed the photovoltaic characteristics as well as the series resistance (Rs) and

shunt resistance (Rsh) for the champion devices based on the reference film and the target film respectively. The devices prepared with PEDOT:PSS additives shown a clear improved PCE reaching a maximum performance 17.56% (at 1.5 v% PEDOT:PSS doping) over the 14.58% champion device efficiency obtained without the use of PEDOT:PSS dopants.

Also, we noted that the improved Voc from 0.96 to 0.99V and Jsc from 20.65 to 22.4 mA/cm2 as shown in the Table 1. With the increasing doping (0%, 0.5%, 1.0%, 1.5%, 2.0% v respectively) of PEDOT:PSS in perovskite the FF improved from 73.3% to 78.7%. At the same time, there is a reduction in series resistance (Rs) while the improvement in shunt resistance (Rsh) for the devices with the $CH_3NH_3PbI_{3-x}Cl_x$-PEDOT:PSS film. Fig. S3 showed the relative changes of these key parameters for 100 cells (20 cells for each batch) with a doping of volume ratio of PEDOT:PSS added into the perovskite film layer. The Voc (Fig. S3b) and Jsc shows improvement from 0.96 to 0.99 V and 20.33 to 22.01 mA/cm2 respectively with the increasing volume ratio of 0 v% to the volume ratio of 1.5 v%, but slightly reduced in the volume ratio of 2.0 v% though it was still higher compare to the 0 v% PEDOT:PSS ratio. The Jsc (Fig S3c) and FF (Fig S3d) showed about the same tendency with the volume ratio of PEDOT:PSS increasing and reached the highest value on the volume ratio of 1.5 v% PEDOT:PSS doping. The improved Jsc, Voc

and FF at 1.5 v% PEDOT:PSS doping resulted into the improved PCE of 16.69%.

Photo absorber layer	Voc (V)	Jsc (mA/cm^2)	FF (%)	PCE (%)	Rs (Ω)	Rsh (kΩ)
$CH_3NH_3PbI_{3-x}Cl_x$:PEDOT:PSS (0 v%)	0.96	20.65	73.3	14.58	116.8	19.9
$CH_3NH_3PbI_{3-x}Cl_x$:PEDOT:PSS (0.5 v%)	0.97	21.08	74.2	15.21	96.8	23.8
$CH_3NH_3PbI_{3-x}Cl_x$:PEDOT:PSS (1.0 v%)	0.98	21.86	76.4	16.45	76.4	25.3
$CH_3NH_3PbI_{3-x}Cl_x$:PEDOT:PSS (1.5 v%)	0.99	22.4	78.7	17.56	59.18	34.3
$CH_3NH_3PbI_{3-x}Cl_x$:PEDOT:PSS (2.0 v%)	0.98	21.57	75.8	16.02	82.4	21.4

Table 1 Photovoltaic performance at 1000 Wm^{-2} (AM1.5G) of PSCs prepared with using pure perovskite; perovskite doped with 0, 0.5, 1.5 and 2 v% PEDOT:PSS. All measurements were done on devices with mask size of 0.150 cm^2 at constant scan speed of 10 mVs^{-1}.

To further confirm the current density increase in the Jsc that resulted in an enhancement of PCE of the devices based on the target sample, the IPCE was recorded and is shown in Fig. 2b. The stronger spectral response in the range from 300 to 550 nm was observed for the

devices prepared based on the control film (1.5 v% PEDOT:PSS doping) as compare to the devices prepared without doping. The integrated current density of 22.23 mA/cm^2 calculated from IPCE was good match with the current density of 22.4 mA/cm^2 obtained from J-V measurement. The increase of IPCE was related with the increase of absorption intensity (Zarazúa et al., 2017) as was recorded in Figure. S4 for the different volume ratios of the PEDOT:PSS additives (0 v%, 0.5 v%, 1.0v%, 1.5 v%, and 2.0 v%). The intensity of absorption in the range from 350 to 550 nm corresponding to IPCE spectra of the target film was stronger than for the control film (Sidhik et al., 2017).

Moreover, water present in perovskite is also passivating the perovskite crystals and the overall growth of the good quality crystals are restricted. To further understand the effect of H_2O. We prepared three type of devices based on different perovskite films as : a) pure perovskite b) perovskite doped with 1.5 v% PEDOT:PSS c) perovskite doped with 1.5 v% H_2O. From the Fig. S2, Table S1. The power conversion efficiency of devices with 1.5v% PEDOT:PSS additives showed the highest efficiency statistics yielding champion performance of 17.56% power conversion efficiency (PCE) with improved photovoltaic characteristics (Voc = 0.99 V, Jsc = 22.34 mA/cm^2, FF=78.8). The performance of the devices with 1.5 v% H_2O additives yielding 15.42% (Voc = 0.97 V, Jsc = 21.19 mA/cm^2, FF = 74.5) PCE for champion device. This indicated the presence of a little H_2O

could effectively enhance the device performance, as compared to the devices with pure perovskite (without doping) that gave 14.69% PCE for champion device (Voc = 0.96 V, Jsc = 20.55 mA/cm^2, FF=73.8). This maybe the increased solubility of perovskite in the solvent and the lower boiling point of water to induce the crystallization of perovskite to be the smoother and continuous films with larger crystals(Heo et al., 2014). Although, the presence of water in excess amount can also influence the growth of superior quality perovskite films (Liu et al., 2017a), adequate amount of water additives was shown to improve the band gap and crystal quality of perovskite films (Zhu et al., 2018). This experiment clearly demonstrated that PEDOT:PSS doped perovskite has potential to improve the performance of solar cells.

To understand this improvement in the device performance obtained on PEDOT:PSS doping. The Electrochemical Impedance Spectroscopy (EIS) is employed, EIS is capable of providing useful information like the series resistance (Rs) , shunt resistance (Rsh) and recombination resistance (Rrec) of the solar cell devices (Shao et al., 2016). According to the previous report (Juarez-Perez et al., 2014), the Rs contributed to wires, substrate and additional contributions could exert an impact on FF that to plays a significant role role in the hole-selective contact in the corresponding devices. As shown in the Fig. 2c. The EIS measurement was monitored at the frequency range from 10^6 to 1 Hz

with an AC amplitude of 0.1V at 0.89V bias under dark conditions. The parameters of Rs and Rsh were obtained from EIS analysis with an equivalent circuit, as shown in the illustration containing a resistance R2 and capacitance C1 in parallel and then in series with the other resistance R1 (Liu et al., 2017b). A lower Rs (59.18 Ω) and higher Rsh (34.3 kΩ) value obtained for the PEDOT:PSS doped films is well-matched with the JV measurements. The corresponding changes were shown in Fig. S3 (e) and (f). Meanwhile, we can observed in Fig. 2c, the Rrec of PSCs increased from 17.5 kΩ to 24.5kΩ then decreased to 21.6kΩ when the PEDOT:PSS additives volume ratio increased from 0 v% to 2.0v% and reached the maximum values at the volume ratio of 1.5v%. These improvements are the result of doping PEDOT: PSS into photosensitive layer that can decrease the recombination at the interface of perovskite and PEDOT:PSS layer to promote the charge transfer and reduce the Rs to increase the FF and Jsc (Ren et al, 2017). Fig. 2d shows that the dark current of devices without (0 v%) and with (1.5 v%) PEDOT: PSS additives. During the operating conditions there is also a charge carrier loss through the leakage pathways and recombination of the free carriers (Unger et al., 2014). To evaluate the charge carrier loss and recombination of the free carrier dark current measurements operated under dark conditions with the different inverted bias voltages were performed. This showed that the dark current density of target sample

was lower than that of the reference sample. Indicating a less charge carrier loss for the devices based on perovskite film with PEDOT: PSS (1.5 v%) additives (Zhang et al., 2017).

3.2 The effect of PEDOT: PSS additives on the perovskite film

The morphology of perovskite film exhibited a great effect on the performance of corresponding devices such as pinholes, voids and coverage (Liu et al., 2017; Jain et al., 2016a, 2016b; Eperon et al., 2014). The growth process of perovskite film also started with the evaporating of the mixed element of solvents, excess organic solvents and the crystallization to the ABX_3 structure with the morphology of less pinholes, voids and good coverage (Ren et al, 2017; Zeng et al, 2017; Ren et al, 2018). The good quality perovskite formed as a result of evaporation of the excess amount of organic component from the original film with the increased annealing time (Zhang et al., 2015). It is observed that for targeted films prepared with 1.5 v% PEDOT:PSS doping the surface morphology of perovskite film and film coverage improved homogeneously resulting into crystalline grains of 1 ɯm average size. Further increasing of doping (2.0 v%) leads to formation of larger crystals with more than >1 ɯm crystal grains. However, the coverage of the film is affected negatively at this step this is due to the excess amount doping of water based PEDOT:PSS which might cause voids in the perovskite film.

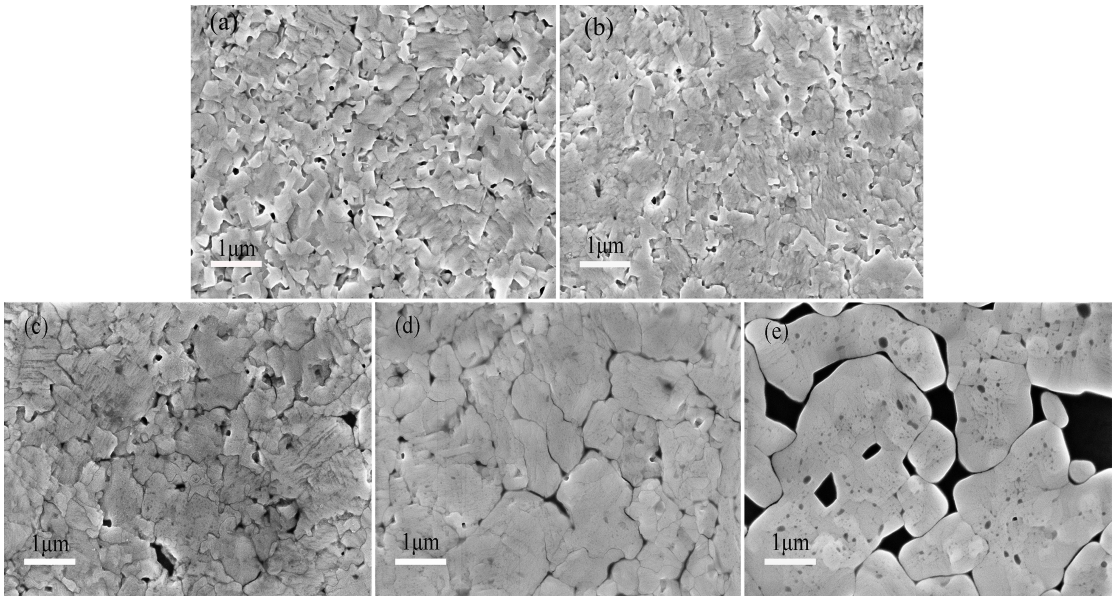

Fig. 3 Top-view FESEM images of $CH_3NH_3PbI_{3-x}Cl_x$-PEDOT:PSS films with the different volumes (0 v%, 0.5 v%, 1.0v%, 1.5 v%, and 2.0 v%) of PEDOT:PSS additives.

Photoabsorber layer	Peak Intensity		FWHM	
	(110)	(220)	(110)	(220)
$CH_3NH_3PbI_{3-x}Cl_x$:PEDOT:PSS (0 v%)	23183	15027	0.117	0.195
$CH_3NH_3PbI_{3-x}Cl_x$:PEDOT:PSS (0.5 v%)	25146	18988	0.108	0.184
$CH_3NH_3PbI_{3-x}Cl_x$:PEDOT:PSS (1.0 v%)	25958	18835	0.104	0.187
$CH_3NH_3PbI_{3-x}Cl_x$:PEDOT:PSS (1.5 v%)	30010	27339	0.100	0.175
$CH_3NH_3PbI_{3-x}Cl_x$:PEDOT:PSS (2.0 v%)	39603	31503	0.095	0.162

Table 2 Peak intensity and FWHM of $CH_3NH_3PbI_{3-x}Cl_x$-PEDOT:PSS films with different volumes of the PEDOT:PSS additives.

Fig. 3 (a-e) shows the FESEM images of $CH_3NH_3PbI_{3-x}Cl_x$-PEDOT:PSS film with the different volumes of PEDOT:PSS additives (0 v%, 0.5 v%,

1.0v%, 1.5 v%, and 2.0 v%). Fig. 3(a) shows the control film that exhibits many small pin-holes and voids. These small pin-holes and voids exerted a lot of change when the different volume ratio of PEDOT:PSS introduced into photosensitive layer. The target film Fig. 3 (d) shown less pin holes and voids, suggesting the better coverage than control film. It is clearly seen that the crystal grain sizes of the target film was much bigger than the control film. According to previous works, Nayak and coworkers changed the acidity of solution to dissolve the colloids, leading to the increasement of free ions concentration in perovskite precursor solution to facilitate the crystallization of resulting film (Nayak et al, 2016). Gong and coworkers added moderate water to the perovskite precursor solution to control the growth of crystalline of perovskite film (Gong et al, 2015). The difference between morphology and quality of these perovskite films showed that PEDOT:PSS as additives had a great impact on the crystallization of the perovskite films due to the acidic nature of PEDOT:PSS aqueous solution and the exist of H_2O components (Noel et al, 2018; Liu et al, 2017a). From XRD (Fig. S5) the strong diffraction peaks at about 14.1º and 28.4º, coming from (110) and (220) lattice plane, which is consistent with the diffraction of crystal planes of the perovskite structure the increased in intensity of the XRD peaks at 14.1º and 28.4º for perovskite doped with PEDOT:PSS. This further, confirmed the better quality of perovskite films obtained as a result of the function of

PEDOT:PSS in the crystallization process of $CH_3NH_3PbI_{3-x}Cl_x$-PEDOT:PSS film (Dong et al., 2017; Dar et al., 2015). Moreover, there are no other impurity phases in the XRD patterns, because of a little presence of PEDOT:PSS as the additives into perovskite active layer and and its presence in X-ray amorphous form. The XRD pattern of PEDOT:PSS film and ITO substrate shown in Fig. S6. This suggested that PEDOT:PSS as the additives didn't have a severe impact with the perovskite crystal phases. Meanwhile, as shown in the Table 2, different peak intensities and full width of half maximum (FWHM) of peaks confirmed the catalytic role played by PEDOT:PSS additives to the crystallization of $CH_3NH_3PbI_{3-x}Cl_x$-PEDOT:PSS films. The larger peak intensities and smaller FWHM indicated the better crystallinity and larger crystal sizes was formed in the different $CH_3NH_3PbI_{3-x}Cl_x$-PEDOT:PSS films. Especially, for the film with 1.5 v% PEDOT:PSS additives. The XRD patterns are also in agreement with the SEM images (Figure 3(a-e)) of corresponding films.

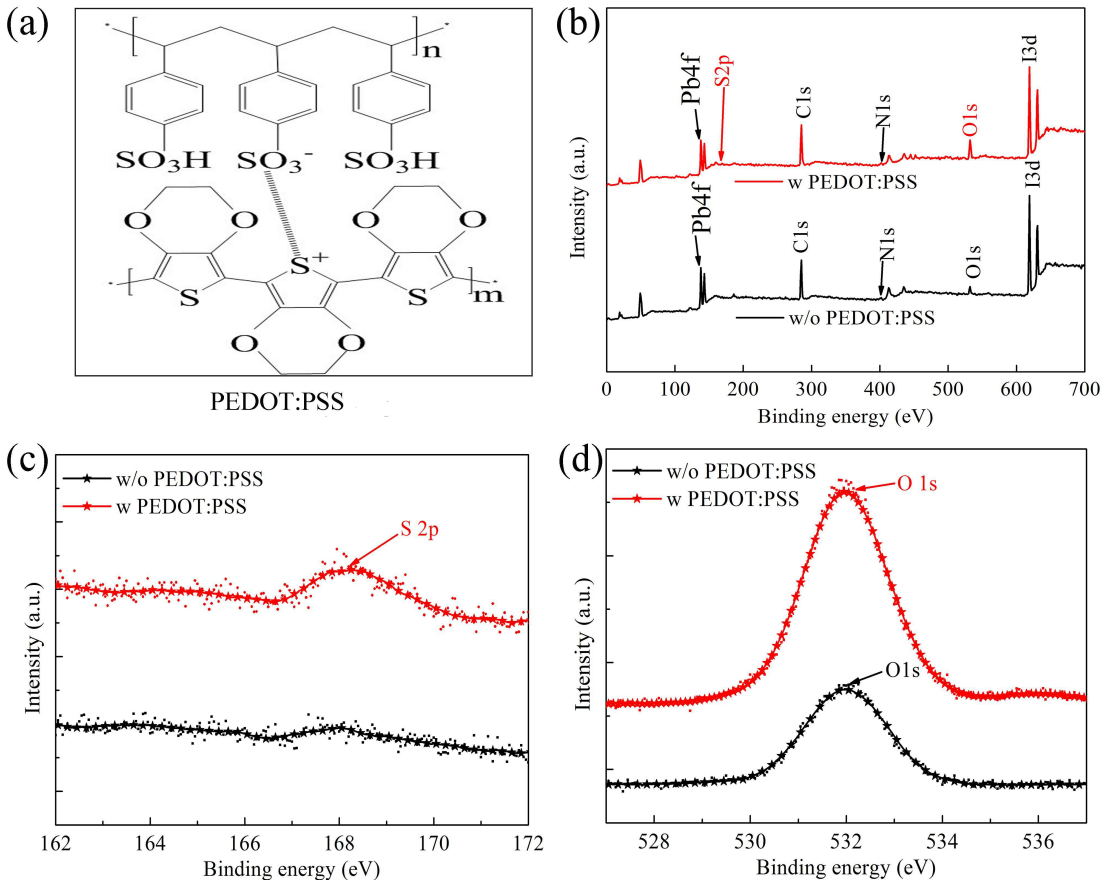

Fig 4. Chemical structure of PEDOT:PSS (a), Overview XPS spectrum of the perovskite film without and with PEDOT:PSS additives (b), Core level S 2P spectrum (c), Core level O 1s spectrum (d).

X-ray photoelectron spectroscopy (XPS) is utilized to understand the role of the PEDOT: PSS dopants in perovskite film. Shown in Fig. 4 (a-d) confirmed the presence of PEDOT: PSS in the $CH_3NH_3PbI_{3-x}Cl_x$:PEDOT:PSS film. Fig. 4 (a-d) shows the peak in 163 to 171 eV and from 530 to 535 eV range. This peak is only observed in the perovskite film with the PEDOT: PSS additives, However, missing or reduced in intensity in the control film. The doublet peak are severally relative to S 2p and O 1s orbitals, which confirmed the successful doping of PEDOT: PSS into the perovskite

film (Andrei et al., 2017; Håkansson et al., 2017). Compared to the control film, the target film has a better coverage that could influence the light absorption of perovskite film and performances of devices. The larger crystal grain sizes in Fig. 3 for the target film exhibited a less grain boundaries to reduce the defects existed in the contact sites between crystal grains than the control. Less boundaries promoted the connectivity of each crystal grain. This has a influence on reducing the energy loss of charge carrier during transport in the perovskite films. To further estimate the hole transport properties of the perovskite films with and without dopants Hole only measurements are performed. Fig. S7 show the current-voltage curve of the device with a hole-only measured using the space-charge limited current (SCLC) model (Chiang and Wu, 2016). The hole-mobility of the devices with PEDOT: PSS doping was higher than the device based on pure perovskite films. Because of the hole conductivity of PEDOT: PSS, the introduction of PEDOT: PSS into photosensitive layer provided more hole transmission channels that lead to improve the transmission of carrier to enhance the Voc (Bi et al., 2016).

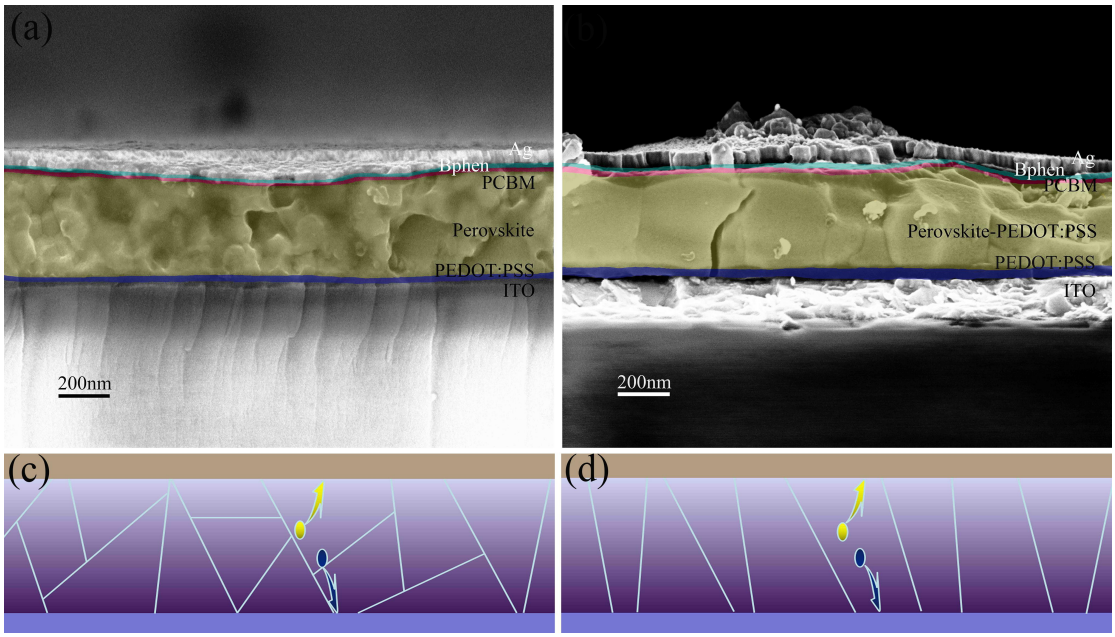

Fig. 5 The cross-section FESEM image of the typical inverted structure of perovskite solar cell (a) without (0 v%) and (b) with the (1.5 v%) PEDOT:PSS additives and the corresponding schematics is represented in (c) and (d).

Fig. 5 (a, b) showed the cross-section FESEM images of the PSC without the (0 v%) and with (1.5 v%) PEDOT: PSS additives and shows the different cross-section morphologies. Interestingly, we observed the target device contained densely packed large grains and more monolithic tendency with vertically oriented crystalline grains that orient from bottom to top while the control device contains loosely packed small grains randomly distributed. The monolithic morphology effectively reduced the defects or trap-states due to the complexation between the uncoordinated Pb atom and the electron-rich of sulfonic acid group in the PEDOT: PSS additive (Noel et al., 2014). According to the previous

literature, because of the halide ions lost in the annealing process and the I-deficient of PbI2. The uncoordinated Pb atoms could act as the electronic trap states in the perovskite films (Noel et al., 2014; Yang et al., 2017; Yin et al., 2014; Jacobsson et al., 2016). We believe the similar happening in our case and the sulfonic acid group in PEDOT:PSS could provide electrons to the uncoordinated Pb atom and form a coordinate band to neutralize the positive Pb atoms (Sun et al., 2016). Moreover, mass loss and surface energy minimization can indirectly determine the final morphology of perovskite films during film formation (Thompson et al., 2012). The complexation could boost the process of crystallization that resulted in a suitable stoichiometry composition to produce a better perovskite film (Shao et al., 2014). The corresponding schematic in Fig 5 (c) and (d) showed the monolithic morphology could produce the larger gains with the better grainy textures that there was nearly perpendicular to horizontal direction to facilitate the charge transfer in the perovskite film (Bai et al., 2017). The $CH_3NH_3PbI_{3-x}Cl_x$-PEDOT:PSS film (1.5 v%) was so dense, homogeneous with an optimized crystal orientation causing to a favorable transfer for the generated electrons or holes through the perovskite layers in a self-transporting mode as previously reported by Heo et al and coworker (Heo et al., 2016). The recombination in the perovskite absorber layer was associated to the defects or trap-states which are dependent on the perovskite film quality.

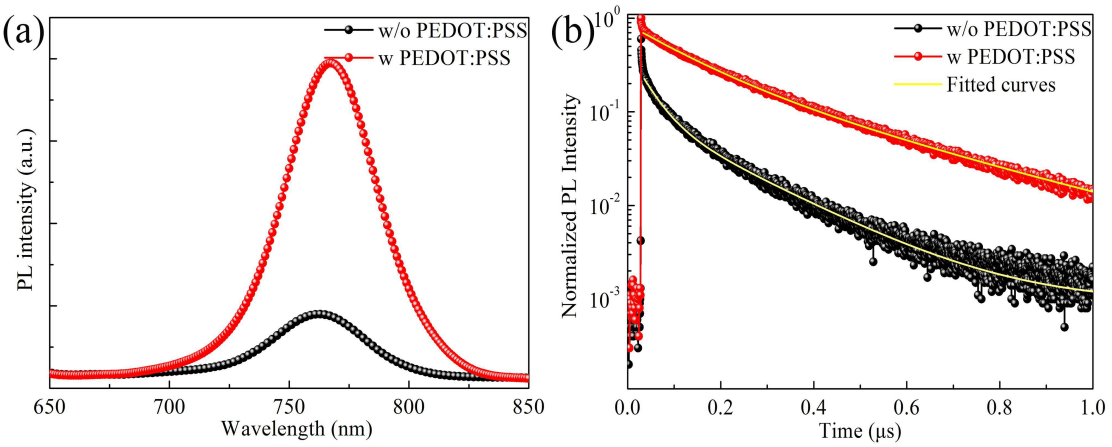

Fig. 6 (a) Steady-state and (b) Time-resolved single photon counting (TCSPC) of $CH_3NH_3PbI_{3-x}Cl_x$-PEDOT:PSS films without (0 v%) and with (1.5 v%) PEDOT:PSS additives.

In order to further explore the role played by PEDOT:PSS doping in the photosensitive layers, the steady-state photoluminescence (PL) and Time correlated single photon counting (TCSPC)was recorded as shown in Fig. 6. For a valid comparison, Perovskite films without and with PEDOT:PSS doing (target film with 1.5%v PEDOT:PSS doping) were spin coated directly on the glass film for photoluminescence measurement. The steady-state PL spectra of control and target films was shown in the Fig. 6(a) in agreement with the reported literature (Wehrenfennig et al., 2014). The perovskite film with PEDOT:PSS doping (red spectrum) shows more than 2 fold increase in intensity as compare to the perovskite films without any dopant (black spectrum). The obvious improvement of the PL spectra intensity in the target film compared to control sample, explained the better crystallization and quality of target film and the significantly reduced non-radiative carrier recombination in target

samples (Ren et al, 2017; Ren et al ,2018; Herz et al., 2016). The non-radiative carrier recombination was also induced with the defects or trap-states in the photosensitive layers (Deschler et al., 2014). Besides, the steady-state PL peak of the target film shift (about 4 nm) towards a long wavelength after inserting the PEDOT:PSS as was seen from Fig. S8, compared to the control film. This phenomenon was consistent with the absorption spectra, and further confirmed the variation of band gap following with the successful introducing of PEDOT:PSS into the perovskite film (Tang et al., 2018) as a result of improved morphology of perovskite crystals. The TCSPC showed in the Fig. 6 (b) shows the decay kinetics between both control and target sample. The solid lines in the plots are well-fitted fluorescence decay spectra with the exponential decay model (Marchioro et al., 2014). The fast relaxation component and long-lasting component was determined to the surface recombination as well the recombination in the bulk of the perovskite structures (Arora et al., 2016). As observed, the PL lifetime of 186 ns of target sample was higher than that for the control sample (86 ns) and is ascribed to the less defects or non-radiative recombination channels in the target sample (Heo et al., 2017). This indicated that a substantive change in the photophysical properties of target film included the slower non-radiative decay rate. In addition, compared with the control film deposited on ITO or on PEDOT:PSS film in Fig. S9, the PL quenching of the target film on

PEDOT:PSS film is conspicuous. It could indicate that with the PEDOT:PSS doping, the target film have a better charge-extraction characteristic to facilitate the charge transfer from the perovskite film to the PEDOT:PSS film (Liu et al, 2018). The favorable crystallization and slow recombination as well as the good charge-extraction characteristic of target film were beneficial to the performance improvement of PSCs.

4. Conclusions

In summary, the classic hole transport material of PEDOT:PSS was used for the first time as an additive within perovskite absorber layer in an inverted perovskite solar cell. After rigorous optimization high quality $CH_3NH_3PbI_{3-x}Cl_x$-PEDOT:PSS films were obtained through the addition of 1.5 v% PEDOT:PSS directly into the perovskite precursor solution. Because of the complexation between the PEDOT:PSS and the target film, the PEDOT:PSS additives shown the following results : (I) improvement of the light harvest of target film as monitored from the UV/Vis absorption spectra that produced more photo generated electron and hole pairs; (II) Improved crystalline quality as confirmed from XRD, Steady state PL, Surface morphology and FEXEM cross-section images that effectively reduce the number of boundaries to decrease the energy loss of carriers during transmission. (III) A monolithic tendency from bottom to top in the cross-section SEM showed that PEDOT:PSS was able to reduce the

defects existed in perovskite film to decrease the recombination rate of carriers. (IV) PEDOT:PSS doping in perovskite not only improved crystalline quality of the films but also showed improved hole extraction capacity of the doped layer and more effective charge extraction as monitored from Hole only mobility measurements and time correlated single photon counting results respectively. All the above improved optoelectronics and device characteristics obtained after PEDOT:PSS doping resulted into the champion devices with power conversion efficiency (PCE) upto 17.56% overtaking the PCE of 14.58% obtained for the devices prepared without any dopants. Overall, this work provides a simple processing via PEDOT: PSS doping directly into perovskite absorber layer as effective route to enhance optoelectronic and photovoltaic properties of perovskite devices for low temperature Inverted perovskite device architecture. Which are closer to commercialization due to their low temperature processing. Our work signifies the importance of this methodology to fabricate devices on flexible substrate and for large scale manufacturing.

Acknowledgements

The authors gratefully acknowledge financial support from the Natural Science Foundation of China (NSFC Grant No. 51502081 and No. 21402042), Henan province natural science foundation (Grant No. 182300410178). S. M. J. acknowledge Marie Curie COFUND fellowship,

Welsh Assembly Government funded Ser-Cymru Solar Project and the Swedish research council (VR) for the financial supports. This project has received funding from the European Union's Horizon 2020 research and innovation programme under the Marie Skłodowska-Curie grant agreement No 663830.

References

Akihiro, K., Kenjiro, T., Shirai, Y., Miyasaka, T., 2009. Organometal Halide Perovskites as Visible-Light Sensitizers for Photovoltaic Cells. J. Am. Chem. Soc. 131, 6050-6051.

Arora, N., Orlandi, S., Dar, M. I., Aghazada, S., Jacopin, G., Cavazzini, M., Mosconi, E., Gratia, P., Angelis, F. D., Pozzi, G., Graetzel M., Nazeeruddin, M. K., 2016. High Open-Circuit Voltage: Fabrication of Formamidinium Lead Bromide Perovskite Solar Cells Using Fluorene-Dithiophene Derivatives as Hole-Transporting Materials. ACS Energy Lett. 1, 107-112.

Andrei, V., Bethke, K., Madzharova, F., Beeg, S., Knop-Gericke, A., Kneipp, J., Rademann, K., 2017. Size Dependence of Electrical Conductivity and Thermoelectric Enhancements in Spin-Coated PEDOT:PSS Single and Multiple Layers. Adv. Electron. Mater. 3, 1600473.

Burschka, J., Pellet, N., Moon, S. J., Humphry-Baker, R., Gao, P., Nazeeruddin, M. K., Grätzel, M., 2013. Sequential deposition as a route to high-performance perovskite-sensitized solar cells. Nature

499, 316-319.

Bai, S., Wu, Z., Wu, X., Jin, Y., Zhao, N., Chen, Z., Mei, Q., Wang, X., Ye, Z., Song, T., Liu, R., Lee, S., Sun, B., 2014. High-performance planar heterojunction perovskite solar cells: Preserving long charge carrier diffusion lengths and interfacial engineering, Nano Res. 12 1749-1458.

Bi, D., Tress, W., Dar, M. I., Gao, P., Luo, J., Renevier, C., Schenk, Abate, K., Giordano, F. , Baena, Juan-Pablo C., 2016. Efficient luminescent solar cells based on tailored mixed-cation perovskites. Sci. Adv. 2, 1501170.

Bai, Y., Xiao, S., Hu, C., Zhang, T., Meng, X., Li, Q., Yang, Y., Wong, K. S., Chen, H., Yang, S., 2017. A pure and stable intermediate phase is key to growing aligned and vertically monolithic perovskite crystals for efficient PIN planar perovskite solar cells with high processibility and stability. Nano Energy 34, 58-68.

Chiang, C., Wu, C., 2016. Bulk heterojunction perovskite-PCBM solar cells with high fill factor. Nature Photonics 10, 196-200.

Chiang, C., Nazeeruddin, M. K., Grätzel, M., Wu C., 2017. The synergistic effect of H_2O and DMF towards stable and 20% efficiency inverted perovskite solar cells. Energy Environ. Sci. 10, 808-817.

Deschler, F., Price, M., Pathak, S., Klintberg, L. E., Jarausch, D.-D., Higler, R., Hüttner, S., Leijtens, T., Stranks, S. D., Snaith, H. J., Atatüre,

M., Phillips, R. T., Friend, R. H., 2014. High Photoluminescence Efficiency and Optically Pumped Lasing in Solution-Processed Mixed Halide Perovskite Semiconductors. J. Phys. Chem. Lett. 5, 1421-1426.

Dar, M. I., Abdi-Jalebi, M., Arora, N., Moehl, T., Grätzel, M., Nazeeruddin, M. K., 2015. Understanding the Impact of Bromide on the Photovoltaic Performance of $CH_3NH_3PbI_3$ Solar Cells Adv. Mater. 27, 7221.

Dong, H., Wu, Z., Xi, J., Xu, X., Zuo, L., Lei, T., Zhao, X., Zhang, L., Hou, X., Jen, Alex K.-Y., 2017. Pseudohalide-Induced Recrystallization Engineering for $CH_3NH_3PbI_3$ Film and Its Application in Highly Efficient Inverted Planar Heterojunction Perovskite Solar Cells. Adv. Funct. Mater. 28, 1704836.

Eperon, G. E., Burlakov, V. M., Docampo, P., Goriely, A., Snaith, H. J., 2014. Morphological Control for High Performance, Solution-Processed Planar Heterojunction Perovskite Solar Cells. Adv. Funct. Mater. 24, 151.

Gong, X., Li M., Shi, X.-B., Ma H., Wang Z.-K., Liao L.-S., 2015. Controllable Perovskite Crystallization by Water Additive for High-Performance Solar Cells. Adv. Funct. Mater. 25, 6671–6678.

Gu, P., Wang, N., Wang, C., Zhou, Y., Long, G., Tian, M., Chen, W., Sun, X. W., Kanatzidis, M. G., Zhang, Q., 2017. Pushing up the efficiency of

planar perovskite solar cells to 18.2% with organic small molecules as the electron transport layer. J. Mater. Chem. A 5, 7339-7344.

Heo, J. H., Song, D. H., Im, S. H, 2014. Planar $CH_3NH_3PbBr_3$ Hybrid Solar Cells with 10.4% Power Conversion Efficiency, Fabricated by Controlled Crystallization in the Spin-Coating Process. Adv. Mater. 26, 8179 – 8183.

Heo, J. H., Lee, M. H., Jang, M. H., Im, S. H., 2016. Highly efficient $CH_3NH_3PbI_{3-x}Cl_x$ mixed halide perovskite solar cells prepared by re-dissolution and crystal grain growth via spray coating. J. Mater. Chem. A. 4, 17636-17642.

Herz, L. M., 2016. Charge-Carrier Dynamics in Organic-Inorganic Metal Halide Perovskites. Annu. Rev. Phys. Chem. 67, 65-89.

Hawash, Z., Raga, S. R., Son, D.Y., Ono, L. K., Park, N.G., Qi, Y. Interfacial Modification of Perovskite Solar Cells Using an Ultrathin MAI Layer Leads to Enhanced Energy Level Alignment, Efficiencies, and Reproducibility. J. Phys. Chem. Lett. 2017, 8, 3947-3953.

Håkansson, A., Han, S., Wang, S., Lu, J., Braun, S., Fahlman, M., Berggren, M., Crispin, X., Fabiano, S., 2017. Effect of (3-glycidyloxypropyl) trimethoxysilane (GOPS) on the electrical properties of PEDOT:PSS films. Journal of Polymer Science Part B: Polymer Physics 55, 814-820.

Heo, S., Seo, G., Lee, Y., Lee, D., Seol, M., Lee, J., Park, Jong-Bong, Kim, K.,

Yun, Dong-Jin, Kim, Y. S., Shin, J. K., Ahn, T. K., Nazeeruddin, M. K., 2017. Deep level trapped defect analysis in $CH_3NH_3PbI_3$ perovskite solar cells by deep level transient spectroscopy. Energy Environ. Sci. 10, 1128-1133.

Hu, L., Sun, K., Wang, M., Chen, W., Yang, B., Fu, J., Xiong, Z., Li, X., Tang, X., Zang, Z., Zhang, S., Sun, L., Li, M., 2017. Inverted Planar Perovskite Solar Cells with a High Fill Factor and Negligible Hysteresis by the Dual Effect of NaCl-Doped PEDOT:PSS. ACS Appl. Mater. Interfaces 9, 43902-43909.

Jeon, N. J., Noh, J. H., Kim, Y. C., Yang, W. S., Ryu, S., Il Seok, S., 2014. Solvent engineering for high-performance inorganic-organic hybrid perovskite solar cells. Nature Materials 13, 897-903.

Juarez-Perez, E. J., Wuβler, M., Fabregat-Santiago, F., Lakus-Wollny, K., Mankel, E., Mayer, T., Jaegermann, W., Mora-Sero, I., 2014. Role of the Selective Contacts in the Performance of Lead Halide Perovskite Solar Cells. J. Phys. Chem. Lett. 5, 680-685.

Jain, S. M., Qiu, Z., Häggman, L., Mirmohades, M., Johansson, M. B., Edvinsson, T., Boschloo, G., 2016a. Frustrated Lewis pair-mediated recrystallization of $CH_3NH_3PbI_3$ for improved optoelectronic quality and high voltage planar perovskite solar cells. Energy Environ. Sci. 9, 3770-3782.

Jain, S. M., Philippe, B., Johansson, Erik M. J., Park, B.-w., Rensmo, H.,

Edvinsson T., Boschloo, G., 2016b. Vapor phase conversion of PbI_2 to $CH_3NH_3PbI_3$: spectroscopic evidence for formation of an intermediate phase. J. Mater. Chem. A. 4, 2630-2642.

Jacobsson, T. J., Correa-Baena, Juan-Pablo, Anaraki, E. H., Philippe, B., Stranks, S. D., Bouduban, M. E. F., Tress, W., Schenk, K., Teuscher, J., Moser, Jacques-E., Rensmo, H., Hagfeldt, A., 2016. Unreacted PbI_2 as a Double-Edged Sword for Enhancing the Performance of Perovskite Solar Cells. J. Am. Chem. Soc. 138, 10331-1343.

Jiang, Q., Chu, Z., Wang, P., Yang, X., Liu, H., Wang, Y., Yin, Z., Wu, J., Zhang, X., You, J., 2017. Planar-Structure Perovskite Solar Cells with Efficiency beyond 21%. Adv. Mater. 29, 1703852.

Kranthiraja, K., Gunasekar, K., Kim, H., Cho, An-Na, Park, Nam-Gyu, Kim, S., Kim, B. J., Nishikubo, R., Saeki, A., 2017. High-Performance Long-Term-Stable Dopant-Free Perovskite Solar Cells and Additive-Free Organic Solar Cells by Employing Newly Designed Multirole π-Conjugated Polymers Song, M. Adv. Mater. 29, 1700183.

Lee, M. M., Teuscher, J., Miyasaka, T., Murakami, T. N., Snaith, H. J., 2012. Efficient Hybrid Solar Cells Based on Meso-Superstructured Organometal Halide Perovskites. Science 338, 643.

Liu, Z., Hu, J., Jiao, H., Li, L., Zheng, G., Chen, Y., Huang, Y., Zhang, Q., Shen, C., Chen, Q., Zhou, H., 2017. Chemical Reduction of Intrinsic Defects in Thicker Heterojunction Planar Perovskite Solar Cells. Adv.

Mater. 29, 1606774.

Liu, Z., He, T., Liu, K., Wang, J., Zhou, Y., Yang, J., Liu, H., Jiang, Y., Ma, H., Yuan, M., 2017a. Efficient and stable perovskite solar cells based on high-quality $CH_3NH_3PbI_{3-x}Cl_x$ films modified by V_2O_x additives. J. Mater. Chem. A 5, 24282-24291.

Liu, Z., He, T., Liu, K., Zhi, Q., Yuan, M., 2017b. Solution processed double-decked V_2O_x/PEDOT:PSS film serves as the hole transport layer of an inverted planar perovskite solar cell with high performance. RSC Adv. 7, 26202-26210.

Liu, Z., He, T., Wang, H., Jain, S. M., Liu K., Yang, J., Zhang, Na, Liu, H., Yuan, M., 2018. Improvement in the performance of inverted planar perovskite solar cells via the $CH_3NH_3PbI_{3-x}Cl_x$:ZnO bulk heterojunction. Journal of Power Sources 401,303-311.

Marchioro, A., Teuscher, J., Friedrich, D., Kunst, M., Krol, R. van de, T. Moehl, T. as, Grätzel, M., Moser, Jacques-E., 2014. Unravelling the mechanism of photoinduced charge transfer processes in lead iodide perovskite solar cells. Nat. Photonics 8, 250-255.

Nayak, P. K, Moore, D. T., Wenger, B., Nayak, S., Haghighirad, A. A., Fineberg, A., Noel, N. K., Reid, O. G., Rumbles, G., Kukura, P., Vincent, K. A., Snaith, H. J., 2016. Mechanism for rapid growth of organic-inorganic halide perovskite crystals. Nature commu. 7, doi: 10.1038/ncomms13303.

Noel, N. K., Abate, A., Stranks, S. D., Parrott, E. S., Burlakov, V. M., Goriely, A., Snaith, H. J., 2014. Enhanced Photoluminescence and Solar Cell Performance via Lewis Base Passivation of Organic-Inorganic Lead Halide Perovskites. ACS NANO 8, 9815-9821.

Noel, N. K., Congiu, M., Ramadan, A. J., Fearn, S., McMeekin, D. P., Patel, J. B., Johnston, M. B., Wenger, B., Snaith, H. J., 2018. Unveiling the Influence of pH on the Crystallization of Hybrid Perovskites, Delivering Low Voltage Loss Photovoltaics. Joule 1, 328-343.

Ren, Y.-K., Ding, X.-H., Wu, Y.-H., Zhu, J., Hayat, T., Alsaedi, A., Xu, Y.-F., Li, Z.-Q., Yang, S.-F., Dai, S.-Y., 2017. Temperature-assisted rapid nucleation: a facile method to optimize the film morphology for perovskite solar cells. J. Mater. Chem. A 5, 20327-20333.

Ren, Y.-K., Shi, X.-Q., Ding, X.-H., Zhu, J., Hayat, T., Alsaedi, A., Li, Z.Q., Xu, X.-X., Yang, S.-F., Dai, S.-Y., 2018. Facile fabrication of perovskite layers with large grains through a solvent exchange approach. Inorg. Chem. Front. 5(2), 348-353.

Shao, Y., Xiao, Z., Bi, C., Yuan Y., Huang, J., 2014. Origin and elimination of photocurrent hysteresis by fullerene passivation in $CH_3NH_3PbI_3$ planar heterojunction solar cells. Nature Commu. 5, DOI: 10.1038/ncomms6784.

Sun, C., Wu, Z., Yip, Hin-Lap, Zhang, H., Jiang, Xiao-Fang, Xue, Q., Hu, Z., Hu, Z., Shen, Y., Wang, M., Huang, F., Cao Y. 2016.

Amino-Functionalized Conjugated Polymer as an Efficient Electron Transport Layer for High-Performance Planar-Heterojunction Perovskite Solar Cells. Adv. Energy Mater. 6, 1501534.

Shao, S., Abdu-Aguye, M., Qiu, L., Lai, Lai-Hung, Liu, J., Adjokatse, S., Jahani, F., Kamminga, M. E., Brink, G. H. ten, Palstra, T. T. M., Kooi, B. J., Hummelen, J. C., Loi, M. A., 2016. Elimination of the light soaking effect and performance enhancement in perovskite solar cells using a fullerene derivative. Energy Environ. Sci. 9, 2444-24.

Sum, T. C., Mathew, N., 2014. Advancements in perovskite solar cells: photophysics behind the photovoltaics. Energy Environ Sci. 7, 2518-2534.

Sidhik, S., Esparza, D., Martínez-Benítez, A., López-Luke, T., Carriles, R., Rosa, E. De la., 2017. Improved performance of mesoscopic perovskite solar cell using an accelerated crystalline formation method. J. Power Sources 365, 169-178.

Thompson, C. V., 2012. Solid-State Dewetting of Thin Films. Ann. Rev. Mater. Res. 42, 399-434.

Tang, Z., Uchida, S., Bessho, T., Kinoshita, T., Wang, H., Awai, F., Jono, R., Maitani, M. M., Nakazaki, J., Kubo, T., Segawa, H., 2018. Modulations of various alkali metal cations on organometal halide perovskites and their influence on photovoltaic performance. Nano Energy 45, 184-192.

Unger, E. L., Hoke, E. T., Bailie, C. D., Nguyen, W. H., Bowring, A. R., Heumuller, T., Christoforo, M. G., McGehee, M. D., 2014. Hysteresis and transient behavior in current-voltage measurements of hybrid-perovskite absorber solar cells. Energy Environ. Sci. 7, 3690-3698.

Wehrenfennig, C., Liu, M., Snaith, H. J., Johnston, M. B., Herz, L. M., 2014. Homogeneous Emission Line Broadening in the Organo Lead Halide Perovskite $CH_3NH_3PbI_{3-x}Cl_x$. J. Phys. Chem. Lett. 5, 1300-1306.

Wu, Y., Yan, D., Peng, J., Duong, T., Wan, Y., Phang, S. P., Shen, H., Wu, N., Barugkin, C., Fu, X., Surve, S., Grant, D., Walter, D., White, T. P., Catchpole, K. R., Weber, K. J., 2017. Monolithic perovskite/silicon-homojunction tandem solar cell with over 22% efficiency. Energy Environ. Sci. 10, 2472-2479.

Wu, Z., Raga, S. R., Juarez-Perez, E. J., Yao, X., Jiang, Y., Ono, L. K., Ning, Z., Tian, H., Qi, 2018. Y. Improved Efficiency and Stability of Perovskite Solar Cells Induced by C=O Functionalized Hydrophobic Ammonium-Based Additives. Adv. Mater. 30, 1703670.

Xie, F., Chen, C.-C., Wu, Y., Li, X., Cai, M., Liu, X., Yang, X., Han, L., 2017. Vertical recrystallization for highly efficient and stable formamidinium-based inverted-structure perovskite solar cells. Energy Environ. Sci. 10, 1942-1949.

Xu, X. Chueh, CC. Yang, Z., Rajagopal, A., Xu, J., Jo, S. B., Jen, A. K.-Y.,

2017. Ascorbic acid as an effective antioxidant additive to enhance the efficiency and stability of Pb/Sn-based binary perovskite solar cells. Nano Energy 34, 392-398.

Xu, X., Ma, C., Cheng, Y., Xie, Y., Yi, X., Gautam, B., Chen, S., Li, H., Lee, C., So, F., Tsang, S., 2017. Ultraviolet-ozone surface modification for non-wetting hole transport materials based inverted planar perovskite solar cells with efficiency exceeding 18%, Journal of Power Sources 360, 157-165.

You, J., Hong, Z., Yang (Michael), Y., Chen, Q., Cai, M., Song, T., Chen, C., Lu, S., Liu, Y., Zhou, H., Yang Y., 2014. Low-Temperature Solution-Processed Perovskite Solar Cells with High Efficiency and Flexibility. ACS NANO 8, 1674-1680.

Yin, Wan-Jian, Shi, T., Yan, Y., 2014. Unusual defect physics in $CH_3NH_3PbI_3$ perovskite solar cell absorber. Appl. Phys. Lett. 104, 063903.

Yang, W. S., Park, Byung-Wook, Jung, E. H., Jeon, N. J., Kim, Y. C., Lee, D. U., Shin, S. Sik, Seo, J., Kim, E. K., Noh, J. H, Seok, S. Il, 2017 Iodide management in formamidinium-lead-halide-based perovskite layers for efficient solar cells. Science 356, 1376-1379.

Zhao, Y., Nardes, A. M., Zhu, K., 2014. Solid-State Mesostructured Perovskite $CH_3NH_3PbI_3$ Solar Cells: Charge Transport, Recombination, and Diffusion Length. J. Phys. Chem. Lett. 5, 490-494.

Zhang, W., Saliba, M., Moore, D. T., Pathak, S. K., Horantner, M. T., Stergiopoulos, T., Stranks, S. D., Eperon, G. E., Alexander-Webber, J. A., Abate, A., 2015. Ultrasmooth organic-inorganic perovskite thin-film formation and crystallization for efficient planar heterojunction solar cells. Nature Commu. 6, doi: 10.1038/ncomms7142.

Zarazúa, I., Sidhik, S., Lopéz-Luke, T., Esparza, D., Rosa, E. De la, Reyes-Gomez, J., Mora-Seró, I., Garcia-Belmonte, G., 2017. Operating Mechanisms of Mesoscopic Perovskite Solar Cells through Impedance Spectroscopy and J-V Modeling. J. Phys. Chem. Lett. 8, 6073-6079.

Zeng, X., Zhou, T., Leng, C., Zang, Z., Wang, M., Hu, W., Tang, X., Lu, S., Fang, L., Zhou, M., 2017. Performance improvement of perovskite solar cells by employing a CdSe quantum dot/PCBM composite as an electron transport layer. J. Mater. Chem. A 5, 17499-17505.

Zhang, H., Wang, H., Chen, W., Jen, A. K.-Y., 2017. $CuGaO_2$: A Promising Inorganic Hole-Transporting Material for Highly Efficient and Stable Perovskite Solar Cells. Adv. Mater. 29, 1604984.

Zhu, Z., Hadjiev, V. G., Rong, Y., Guo, R., Cao, B., Tang, Z., Qin, F., Li, Y. , Wang, Y., Hao, Venkatesan, F. S., Li W., Baldelli S., Guloy, A. M., Fang H., Hu Y., Yao Y., Wang Z., Bao J., 2018. Interaction of Organic Cation

with Water Molecule in Perovskite $MAPbI_3$: From Dynamic Orientational Disorder to Hydrogen Bonding. Chem. Mater. 28, 7385-7393.